Talanta 188 (2018) 708–713

Contents lists available at ScienceDirect

Talanta

journal homepage: www.elsevier.com/locate/talanta

Ratiometric fluorescence sensor based on cholesterol oxidase-functionalized mesoporous silica nanoparticle@ZIF-8 core-shell nanocomposites for detection of cholesterol

Ke Wang[a,1], Hailong Ren[b,1], Nan Li[a], Xiaoyan Tan[c], Fuquan Dang[a,*]

[a] Key Laboratory of Analytical Chemistry for Life Science of Shaanxi Province, School of Chemistry and Chemical Engineering, Shaanxi Normal University, 620 West Chang'an Street, Xi'an 710119, China
[b] Sports Institute of Shaanxi Normal University, 620 West Chang'an Street, Xi'an 710119, China
[c] Department of Obstetrics and Gynecology, The Fourth Military Medical University, 169 Changle West Road, Xi'an 710032, China

ARTICLE INFO

Keywords:
Ratiometric fluorescence sensor
Dye packaging
ZIF-8 transition layer
Oxidase-functionalized
Cholesterol detection

ABSTRACT

A novel ratiometric fluorescence sensing system based on cholesterol oxidase-functionalized dual-color mesoporous silica nanoparticles (MSNs)@metal-organic framework core-shell nanocomposite is demonstrated for cholesterol detection. MSNs were first loaded with 5-aminofluorescein (AF) inside pores and then wrapped with red-emission CdTe quantum dots (QDs) on the surface to seal in the dye molecules, forming the signal displaying unit (AF-MSN-QDs). Next, AF-MSN-QDs were encapsulated with zeolitic imidazolate framework (ZIF-8) to form a transition layer with distinct size-selectivity, which not only protected the cores from corrosion but also greatly decreased background interference from large molecules. More significantly, the ZIF-8 shells showed high affinity for most enzymes, which made it possible for cholesterol oxidase (ChOx) to self-organize on the surface of ZIF-8-encapsulated AF-MSN-QDs via chemo-physical adsorption, forming novel core-shell nanocomposites (AF-MSN-QD@ZIF-8-ChOx) as a sensing platform for cholesterol detection. The detectable signal was monitored by enzymatic product-quenching fluorescence of the QDs. The fluorescence changes of I_{520}/I_{618} showed excellent linearity with H_2O_2 concentrations in the range of 5–100 nM, with a limit of detection (LOD) as low as 0.89 nM. As a proof-of-concept, cholesterol was selectively detected with beneficial LOD as low as 0.923 μg/mL, demonstrating the great potential of this biosensor platform for other biologically important molecules with H_2O_2-producing oxidases.

1. Introduction

Cholesterol is an important compound in brain and nerve cells; they are precursors of other biological materials, such as steroid hormones and bile acids. Without cholesterol, brain cells cannot send messages that power the organs in our bodies. However, it is essential that the human body maintains cholesterol levels within a certain range [1]. The concentration of cholesterol in human serum should be lower than 200 mg dL^{-1} under normal circumstances, any serum level higher than 240 mg dL^{-1} specifies high blood cholesterol. High cholesterol levels can cause damage to blood vessels and result in arteriosclerosis, cardiovascular diseases, heart disease, cerebral thrombosis, coronary artery disease, and other diseases [2–4]. Meanwhile, a low concentration of cholesterol (< 167 mg dL^{-1}) results in hypocholesterolemia, which may cause hemorrhagic stroke [5]. To date, several biosensor strategies have been proposed for the selective detection of a single analyte in the blood [6,7]. A number of methods have been employed to detect cholesterol, such as high-performance liquid chromatography [8], thin layer chromatography [9], electrochemical methods [10,11], colorimetry [12,13], photonic crystal [14], and fluorescence-based assays [15]. Among these approaches, the fluorescence method is endowed with distinct merits for applications in cholesterol detection assays due to its simplicity, rapidity, sensitivity, spatiotemporal resolution , and wide linear range.

To obtain more accurate readouts, ratiometric fluorescent assays have drawn considerable attention because of their self-calibration. Ratiometric fluorescent assays, which detect the analyte by measuring the change in the ratios of fluorescence intensities at two wavelengths, can achieve improved sensitivity and accuracy by providing built-in correction for environmental conditions [16]. Quantum dots (QDs) are

* Corresponding author.
E-mail address: dangfqn@snnu.edu.cn (F. Dang).
[1] These authors contributed equally to this work and should be considered as co-first authors.

https://doi.org/10.1016/j.talanta.2018.06.019
Received 21 January 2018; Received in revised form 31 May 2018; Accepted 6 June 2018
Available online 15 June 2018
0039-9140/

advantageous over organic fluorophores due to their broad absorption and narrow, size-tunable emission, which enables different-band emissions by single-wavelength excitation [17,18]; thus, QDs are superior for constructing multicolored fluorescent systems [19,20]. In the past few years, ratiometric fluorescent nanoprobes based on dual-color QD systems have been successfully developed for visual and sensitive detection of metal ions [21], TNT [22], amino acids [23], and duplex DNA [24]. Recently, mesoporous silica nanoparticles (MSNs) have been recognized as an intelligent carrier material for a controllable release system because of its unique pore size, large load capacity, chemical and thermal stability, and fine dispersibility in aqueous solutions. Moreover, MSNs with high surface silanol groups are conducive to various surface reactions and the bonding of biomolecules [25]. On the other hand, metal–organic frameworks (MOFs) have attracted considerable research attention on account of their high ordered crystalline porous networks; high pore volume, and high specific surface area [26]. Recently, MOFs were expanded by encapsulating nanoparticles (NPs) within MOFs, forming core-shell NP@MOF nanocomposites. The NP@MOF nanocomposites are of great interest because it provides MOFs and certain classes of NPs with novel chemical and physical properties, including photoluminescence properties, tunable porosity, and higher surface area [27]. Since the surface unsaturated ligand metals of MOFs may be favorable for the high affinity binding of enzymes via coordinative bonds, we hypothesize that core-shell NP@MOF nanocomposites can be utilized as a promising platform for facile enzyme immobilization via chemo-physical adsorption, and thus for the construction of enzyme-based biosensors.

Herein, a novel ratiometric fluorescence sensing system based on cholesterol oxidase-functionalized dual-color MSN@MOF core-shell nanocomposites is developed for the detection of cholesterol. We demonstrate the rational synthesis of dual-color MSN@MOF core-shell nanocomposites and their first used as substrate for enzyme immobilization. The synthetic route is showed in Scheme 1. Firstly, MSNs were synthesized using a sol-gel method, and then 5-aminofluorescein (AF) was encapsulated inside the MSN pores. The AF-MSN surface was grafted with CdTe QDs, resulting in dual-color AF-MSN-QD nanocomposites. Secondly, a zeolitic imidazolate framework (ZIF-8) transition layer was deposited on the surface of the AF-MSN-QD nanocomposites, granting size-selectivity, anti-interference properties, chemical and thermal stability, and fine dispersibility to the nanocomposites. Afterward, the cholesterol oxidase (ChOx) was tightly immobilized on the surface of ZIF-8 shells via coordinative bonds intact by copious phosphate buffer saline (PBS, 10 mM, pH 7.4). Finally, H_2O_2 produced in the presence of cholesterol readily permeated through the shell of ZIF-8 and then quenched the fluorescence of the CdTe QDs, whereas cholesterol and cholestenone have little influence on AF-MSN-QD@ZIF-8 fluorescence. Hence, the highly sensitive detection of cholesterol was completed by observing the fluorescence ratio of I_{520}/I_{618} (I_{520} and I_{618} are the fluorescence intensity of AF-MSN-QD@ZIF-8-ChOx at 520 and 618 nm, respectively) by H_2O_2 produced in the presence of cholesterol.

2. Results and discussion

2.1. Characterization of AF-MSN-QD@ZIF-8

To construct a target dye loading system, the successful synthesis of MSNs with porous structures is crucial. As shown in Fig. 1A, MSNs were synthesized as described in literature [28], in which the average diameter of the MSNs was ≈ 70 nm and the average pore diameter was ≈ 2.7 nm. The pore size is large enough for loading fluorescent dye. The AF-MSN exhibits a significantly different morphology as compared to that of the MSNs, indicating the successful encapsulation of the dye inside of MSN (Fig. 1B). In contrast, the TEM image of QD-capped MSNs shows dark spots of about 6 nm in diameter on the exterior of the MSNs, indicating aggregation of the QDs on the exterior of the MSNs (Fig. 1C). The CdTe QDs of AF-MSN-QDs nanocomposites synthesized herein was composed of multiple QDs with almost identical morphologies to the native QDs (Fig. S1). The TEM characterization revealed a well-defined core–shell structure with an AF-MSN-QD core and a ZIF-8 shell of ≈ 31 nm in thickness, which provided clear evidence of the successful wrapping of AF-MSN-QDs with the ZIF-8 shell (Fig. 1D). The ZIF-8 shell not only protects cores from corrosion, but also greatly decreases background interference from large molecules, and further provides a platform for facile enzyme immobilization.

FTIR spectroscopy was performed to further investigate the structures of the MSNs, AF-MSNs, and AF-MSN-QDs. MSN-NH_2 gave a typical FTIR spectrum with a large band at 3100–3500 cm^{-1} due to the O-H stretching vibration, two peaks at 795 and 1090 cm^{-1} due to the Si-O symmetric and asymmetric vibrations, a peak at 950 cm^{-1} assigned to the Si-OH asymmetric vibration, and at 1520 cm^{-1} due to the N-H bending vibration, consistent with published data (Fig. S2, black

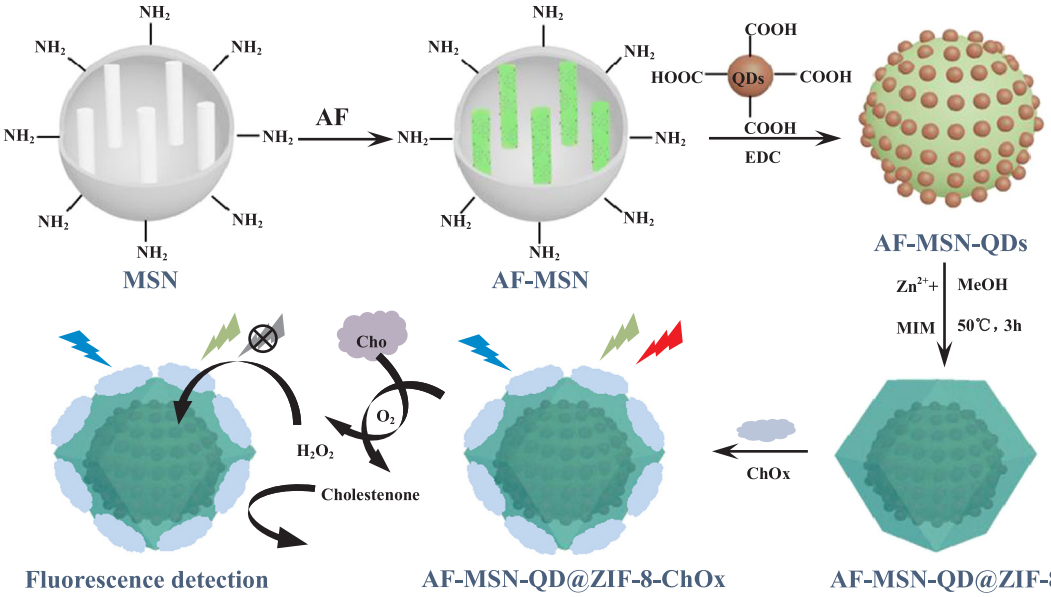

Scheme 1. The synthetic route to AF-MSN-QD@ZIF-8 with the enzyme immobilization and ratiometric fluorescence strategy based on AF-MSN-QD@ZIF-8-ChOx for cholesterol detection.

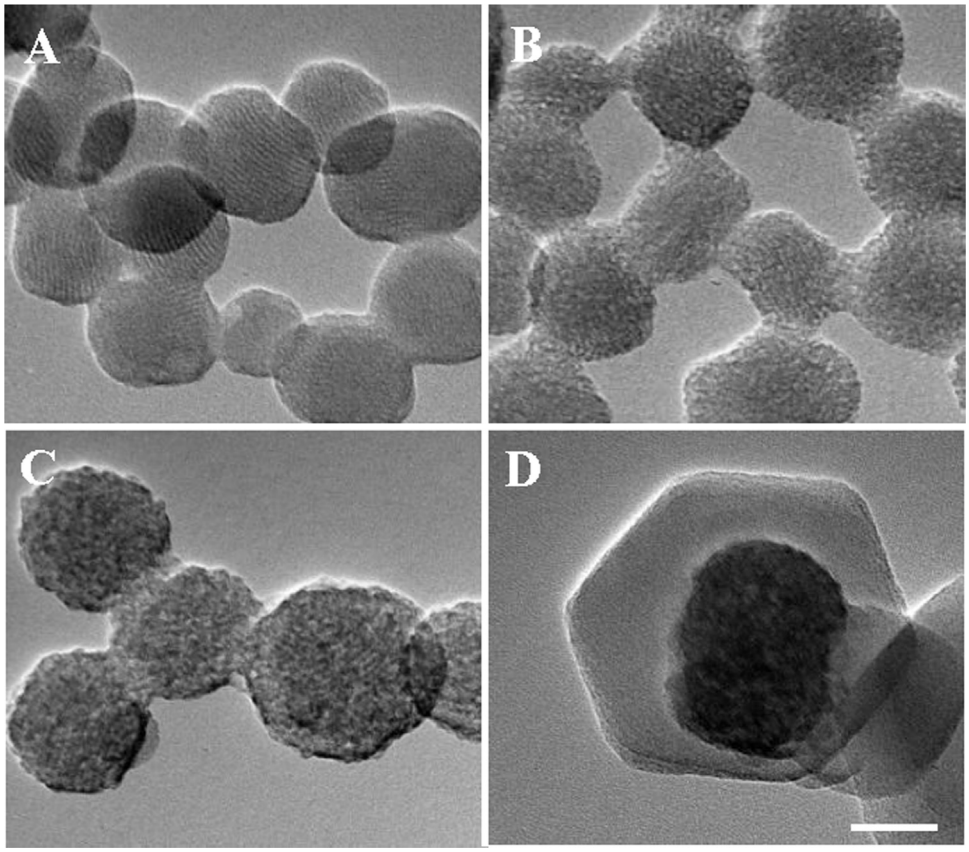

Fig. 1. TEM images of (A) APTES-modified MSNs (MSN-NH_2), (B) AF-MSNs, and (C) AF-MSN-QDs, (D) AF-MSN-QD@ZIF-8. Scale bar: 50 nm.

line) [29]. AF-MSNs showed similar characteristic peaks to those of MSNs, except for additional peaks at 1395–1440 cm^{-1} and 1470 cm^{-1} from C-O and C=C stretching vibrations, respectively, which can be explained by the AF (Fig. S2, red line), indicating successful encapsulation of AF in the MSN porous structures. Once the AF-MSN-NH_2 reacted with the COOH-QDs, a characteristic band at 1562 cm^{-1} attributed to the CO-NH vibration indicated the successful conjugation of QDs on the exterior surface of AF-MSNs (Fig. S2, blue line). Moreover, the decoration of the ZIF-8 on the above AF-MSN-QDs is confirmed by the presence of 6.62 at% Zn^{2+} in EDX analysis (Fig. S3).

To demonstrate the mechanism of AF-MSN-QD@ZIF-8 fluorescence quenching by H_2O_2, the optical properties of AF, QDs, and AF-MSN-QD@ZIF-8 were investigated. Fig. 2A shows that the AF and QDs have a characteristic peak at 520 nm and 618 nm, respectively, while AF-MSN-QD@ZIF-8 exhibits two characteristic peaks at 520 nm and 618 nm. Varying the excitation wavelength from 420 to 460 nm at 10 nm intervals showed that the AF-MSN-QD@ZIF-8 PBS solution exhibited almost the same fluorescence emission peaks at 520 nm and 618 nm upon excitation at 440 nm (Fig. 2B). The lack of changes in the fluorescence of AF before and after adding H_2O_2 excluded the possibility that H_2O_2 directly changed the fluorescence of AF (Fig. S4A). In contrast, the fluorescence of the QDs at 618 nm gradually decreased with increasing H_2O_2 concentration from 0 to 10 μM (Fig. S4B), indicating that the correlation between fluorescence intensity and H_2O_2 concentration was dose-dependent.

2.2. Ratiometric fluorescent detection of H_2O_2

Fig. S5 shows the relationship between the AF-MSN-QD@ZIF-8 concentration and the fluorescence quenching effect on the QDs, $(I_0\text{-}I)/I_0$, where I_0 and I represent the fluorescence intensities at 618 nm before and after the addition of 50 nM H_2O_2 to the AF-MSN-QD@ZIF-8

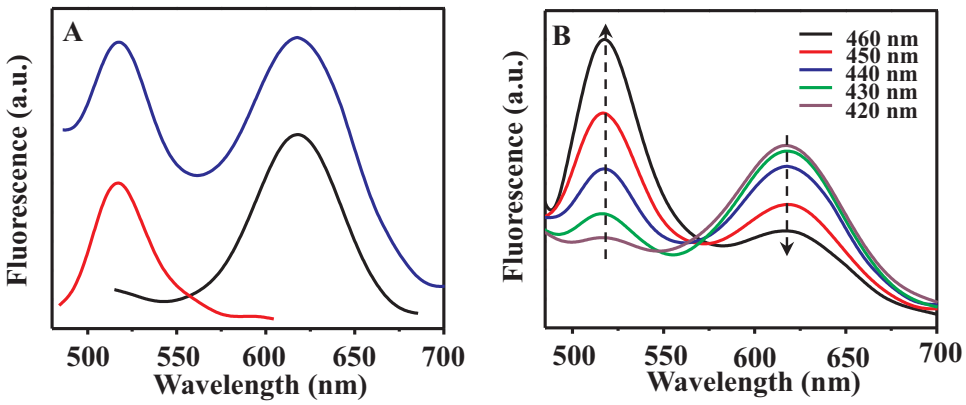

Fig. 2. (A) Fluorescent emission spectra of AF with the characteristic peak at 520 nm (red line) upon excitation at 460 nm; QDs with the characteristic peak at 618 nm (black line) upon excitation at 420 nm, and AF-MSN-QD@ZIF-8 with two characteristic peaks at 520 and 618 nm (blue line) upon excitation at 440 nm. (B) Emission spectra of AF-MSN-QD@ZIF-8 at excitation wavelengths from 420 to 460 nm at intervals of 10 nm.

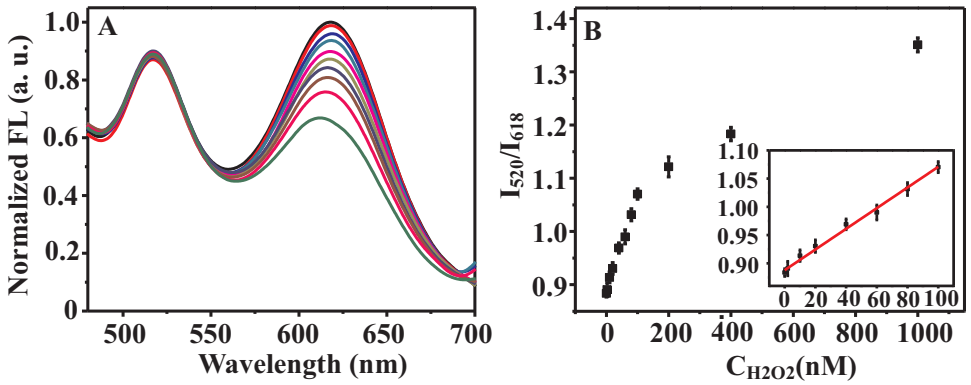

Fig. 3. (A) Fluorescence emission changes with increased H_2O_2 concentrations (0, 5, 10, 20, 40, 60, 80, 100, 200, 400, and 1000 nM). (B) The linear relationship of H_2O_2 concentration from 0 to 1000 nM and the ratiometric fluorescence intensity I_{520}/I_{618}. Inset: plot of linear region from 0 to 100 nM.

solution, respectively. The quenching effects of H_2O_2 on QDs were studied in the concentration range 0.6–1.0 mg/mL. By harmonizing the quenching effect and incubation time, an AF-MSN-QD@ZIF-8 concentration of 0.8 mg/mL was chosen for determining the H_2O_2 quenching effect. Using the optimal experimental conditions obtained above, the linear response of the reaction system to H_2O_2 concentrations ranging from 0 to 100 nM was evaluated. As shown in Fig. 3A, the ratiometric fluorescence intensity I_{520}/I_{618} of AF-MSN-QD@ZIF-8 was gradually enhanced with increasing H_2O_2 concentrations from 0 to 1000 nM, indicating that the relationship between the ratiometric fluorescence intensity I_{520}/I_{618} and H_2O_2 concentration is dose-dependent. The inset of Fig. 3B shows the calibration curves based on the ratiometric fluorescence intensity I_{520}/I_{618} versus H_2O_2 concentration. In the linear region (2, 10, 20, 40, 60, 80, and 100 nM), the regression equation is $y = 0.001820x + 0.8888(R^2 = 0.9923)$, with a limit of detection (LOD) as 0.89 nM (3σ/ slope, where σ is the standard deviation of the blank samples). It is noteworthy that our assay provided a lower detection limit than the previously reported methods for H_2O_2 detection [30–37]. Therefore, cholesterol detection using the H_2O_2-dependent signal from ChOx-catalyzed cholesterol is feasible.

2.3. Ratiometric fluorescent detection of cholesterol

An enzymatic reaction of cholesterol that produced H_2O_2 was detected. The mechanism for the ChOx enzymatic reaction is as follows:

$$\text{Cholesterol} + O_2 \xrightarrow[ChOx]{} \textit{Cholestenone} + H_2O_2$$

The surface unsaturated coordination Zn^{2+} in the ZIF-8 is favorable for efficient binding of ChOx via coordinative bonds, which makes immobilization of ChOx on the surface of AF-MSN-QD@ZIF-8 by a physical adsorption method possible. Expectedly, ChOx readily self-organized onto the ZIF-8 surface to form robust AF-MSN-QD@ZIF-8-ChOx nanocomposites, which is washed with phosphate buffered saline solution (PBS, 10 mM, pH 7.4) and showed a sharp response to cholesterol. The reaction time of the ChOx-mediated enzymatic reaction and the amount of AF-MSN-QD@ZIF-8-ChOx were then investigated to obtain optimum conditions. Fig. S6A shows the relationship between the AF-MSN-QD@ZIF-8-ChOx concentration and the fluorescence quenching effect on the QDs, $(I_0\text{-}I)/I_0$, where I_0 and I represent the fluorescence intensities at 618 nm before and after the addition of cholesterol to the AF-MSN-QD@ZIF-8 solution, respectively. The quenching effects of cholesterol on QD fluorescence intensity was studied in the concentration range 0.3–0.8 mg/mL. By harmonizing the quenching effect and incubation time, an AF-MSN-QD@ZIF-8-ChOx concentration of 0.5 mg/mL was chosen for determining the cholesterol quenching effect. Fig. S6B shows that the hydrolysis of cholesterol by ChOx gradually increases with increasing incubation time, during which the fluorescence spectra was recorded every 10 min, and an equilibrium point was reached within 30 min. Balancing the quenching effect and time consumption, an incubation time of 30 min was chosen for the quantitative determination of the cholesterol quenching effect. The sensitivity of ChOx-mediated cholesterol detection was evaluated using the above optimum conditions. A gradual decrease in the fluorescence intensity at 618 nm was studied in the cholesterol concentration range from 0 to 100 μg/mL (Fig. 4A). Because of H_2O_2 production from the ChOx-assisted oxidation of cholesterol, the fluorescence ratio gradually increased with increasing cholesterol concentration, displaying a cholesterol dose-dependent fluorescence ratio enhancement. Fig. 4B shows a plot of I_{520}/I_{618} versus cholesterol concentration. The response is linear in the range of 0–10 μg/mL cholesterol. The linear equation is $y = 0.01230\times + 0.9184$, and $R^2 = 0.9942$. The limit of

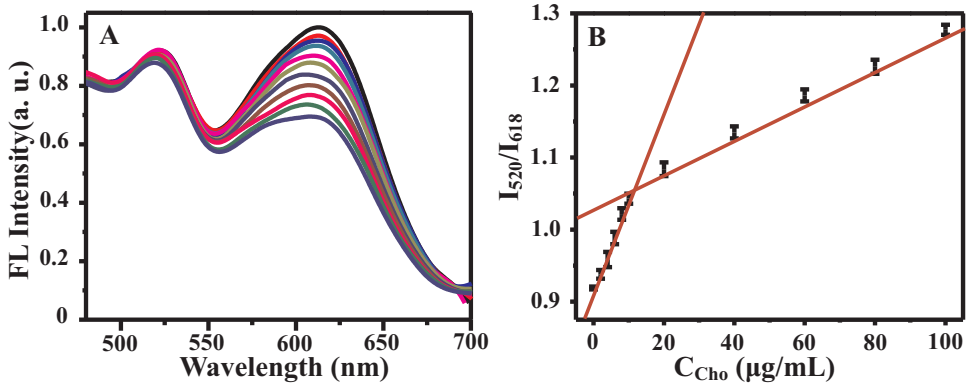

Fig. 4. (A) Ratiometric fluorescent responses of AF-MSN-QD@ZIF-8-ChOx to different concentrations of cholesterol (0, 2, 4, 6, 8, 10, 20, 40, 60, 80, and 100 μg/mL). (B) The linear relationship of cholesterol concentrations from 0 to 100 μg/mL and the ratiometric fluorescence intensity.

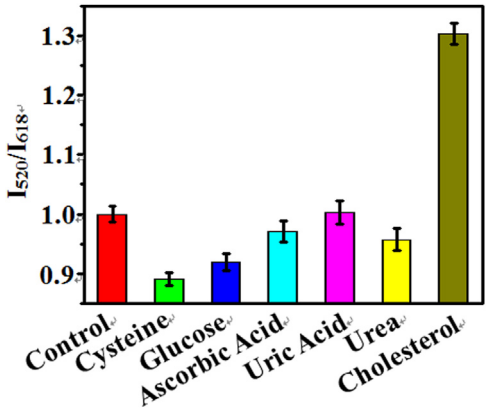

Fig. 5. Selectivity investigation of the proposed method for detection of cholesterol.

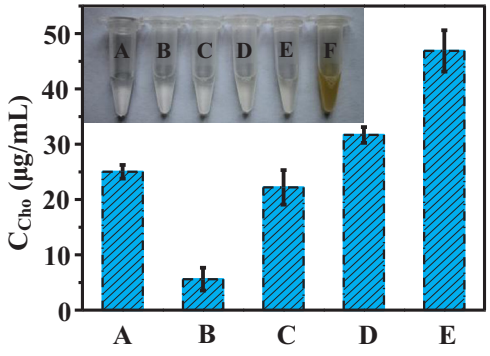

Fig. 6. The cholesterol concentration for blank (A) and diluted serum samples (B–E). Inset: corresponding photographs of the colored supernatant of reaction mixtures. (A, 25 μg/mL of cholesterol; B, serum diluted 200 times; C, serum diluted 50 times; D, serum diluted 200 times with 25 μg/mL of cholesterol; E, serum diluted 50 times with 25 μg/mL of cholesterol; F, serum sample.).

detection of cholesterol was calculated to be 0.9230 μg/mL (3σ/ slope, where σ is the standard deviation of the blank samples). The response is linear in the range of 10–100 μg/mL cholesterol. The linear equation is $y = 0.002550\times + 1.026$, $R^2 = 0.9929$. The detection sensitivity for cholesterol was higher than other nanomaterials. A comparison with previous methods for cholesterol detection is shown in Table S1. The AF-MSN-QD@ZIF-8-ChOx assay is more sensitive than a number of reported approaches involving nanomaterials, but not more sensitive than the methods based on Au nanoparticles [38].

2.4. Selectivity test

We next examine its efficacy in selective cholesterol detection in the complicated system of human serum, which has a multitude of interference from the simultaneous presence of urea, uric acid, cysteine, glucose, and ascorbic acid (commonly present in blood, respectively at 1 mM). For this investigation, 100 μg/mL of cholesterol and 2 mM of urea, uric acid, cysteine, glucose, and ascorbic acid was each taken and analyzed for detecting of cholesterol [38]. The results in Fig. 5 clearly demonstrate that the proposed AF-MSN-QD@ZIF-8-ChOx-based system has high selectivity for cholesterol detection.

2.5. Practical application in real samples

The dependability of the results was examined by testing the serum samples. The proposed method was applied to detect cholesterol in different serum samples from healthy volunteers. Serum sample was diluted 50 and 200 times with 10 mM PBS (pH 7.4) before use. As shown in Fig. 6, the system was successfully tested on real human serum samples containing different concentrations of cholesterol, with the optical image showing different the color formations in the inset. These results agreed with those obtained by the conventional enzymatic method with a RSD of 3.0–4.8% (Table S2), indicating great potential of the AF-MSN-QD@ZIF-8-ChOx-based system for analysis of real samples.

3. Conclusions

In summary, a novel ratiometric fluorescence sensing system based on cholesterol oxidase-functionalized dual-color MSN@MOF core-shell nanocomposites have demonstrated for the detection of cholesterol. MSNs were first loaded with AF and then wrapped with red-emission QDs on the surface to seal in the dye molecules, forming the signal-displaying unit of the ratiometric fluorescence sensor. Next, AF-MSN-QDs were encapsulated with ZIF-8 to form a transition layer with distinct size-selectivity, chemical and thermal stability, and fine dispersibility. The ZIF-8 shells not only protect the cores from corrosion but also greatly decrease background interference from large molecules, and further provide an efficient platform for enzyme immobilization. ChOx was readily immobilized on the surface of ZIF-8-encapsulated AF-MSN-QDs via chemo-physical adsorption, forming ratiometric fluorescence sensing system for the highly selective and sensitive detection of cholesterol in both standard solutions and serum samples. The current work demonstrates the great potential of the AF-MSN-QD@ZIF-8 core-shell nanocomposites as a general and promising sensing platform for other biologically important molecules with H_2O_2-producing oxidases.

Acknowledgments

This work was supported by the National Natural Science Foundation of China (No. 21175088).

Appendix A. Supplementary material

Supplementary data associated with this article can be found in the online version at http://dx.doi.org/10.1016/j.talanta.2018.06.019.

References

[1] D. Voet, J.G. Voet, C.W. Pratt, Fundamentals of Biochemistry: Life at the Molecular Level, 4th edn, Wiley, Hoboken, NJ, 2013.
[2] T.T. Bui, S.Y. Park, Green Chem. 18 (2016) 4245–4253.
[3] P.W.F. Wilson, R.B. D'Agostino, D. Levy, A.M. Belanger, H. Silbershatz, W.B. Kannel, Circulation 97 (1998) 1837–1847.
[4] R. Ahmad, N. Tripathy, J.-H. Parkc, Y.-B. Hahn, Chem. Commun. 51 (2015) 11968–11971.
[5] D.N. Orken, G. Kenangil, E. Uysal, L. Gundogdu, E. Erginoz, H. Forta, Clin. Neurol. Neurosurg. 112 (2010) 668–671.
[6] Y.B. Hahn, R. Ahmad, N. Tripathy, Chem. Commun. 48 (2012) 10369–10385.
[7] B.H. Chu, B.S. Kang, C.Y. Chang, F. Ren, A. Goh, A. Sciullo, W. Wu, J. Lin, B.P. Gila, S.J. Pearton, J.W. Johnson, E.L. Piner, K. Linthicum, J. IEEE Sens. J. 10 (2010) 64–70.
[8] W.W. Wong, D.L. Hachey, L.L. Clarke, S. Zhang, M. Llaurador, W.G. Pond, Appl. Radiat. Isot. 45 (1994) 529–533.
[9] S.P. Singh, S.K. Arya, P. Pandey, B.D. Malhotra, Appl. Phys. Lett. 91 (2007) 063901.
[10] X. Lin, Y. Ni, S. Kokot, Sen. Actuators B 233 (2016) 100–106.
[11] S. Nantaphol, O. Chailapakul, W. Siangproh, Sen. Actuators B 207 (2015) 193–198.
[12] N.R. Nirala, S. Pandey, A. Bansal, V.K. Singh, B. Mukherjee, P.S. Saxena, A. Srivastava, Biosens. Bioelectron. 74 (2015) 207–213.
[13] Y. Zhang, Y. Wang, X. Sun, L. Chen, Z. Xu, Sen. Actuators B 246 (2017) 118–126.
[14] Q. Raj, Z. Xie, H. Ding, C. Zhu, Z. Yang, Z. Gu, Small 11 (2015) 5766–5770.
[15] Y. Cheng, P. Jiang, S. Lin, Y. Li, X. Dong, Sen. Actuators B 193 (2014) 838–843.
[16] J.L. Yao, K. Zhang, H.J. Zhu, F. Ma, M.T. Sun, H. Yu, J. Sun, S.H. Wang, Anal. Chem. 85 (2013) 6461–6468.
[17] M.Y. Han, X.H. Gao, J.Z. Su, S.M. Nie, Nat. Biotechnol. 19 (2001) 631–635.
[18] I.L. Medintz, H.T. Uyeda, E.R. Goldman, H. Mattoussi, Nat. Mater. 4 (2005) 435–446.
[19] C.M. Tyrakowski, P.T. Snee, Anal. Chem. 86 (2014) 2380–2386.
[20] M.O. Noor, U.J. Krull, Anal. Chem. 86 (2014) 10331–10339.
[21] L. Wu, Q.S. Guo, Y.Q. Liu, Q.J. Sun, Anal. Chem. 87 (2015) 5318–5323.
[22] S.F. Xu, H.Z. Lu, Chem. Commun. 51 (2015) 3200–3203.
[23] K. Wang, J. Qian, D. Jiang, Z.T. Yang, X.J. Du, K. Wang, Biosens. Bioelectron. 65

(2015) 83–90.
[24] Y.Q. Liu, M.F. Ye, Q.Y. Ge, X.J. Qu, Q.S. Guo, X.Y. Hu, Q.J. Sun, Anal. Chem. 88 (2016) 1768–1774.
[25] P. Zhang, F. Cheng, R. Zhou, J. Cao, J. Li, C. Burda, Q. Min, J. Zhu, Angew. Chem., Int. Ed. 53 (2014) 2371–2375.
[26] T.R. Cook, Y.R. Zheng, P.J. Stang, Chem. Rev. 113 (2013) 734–777.
[27] K. Wang, N. Li, J. Zhang, Z. Zhang, F. Dang, Biosen. Bioelectron. 87 (2017) 339–344.
[28] S. Sreejith, X. Ma, Y. Zhao, J. Am. Chem. Soc. 134 (2012) 17346–17349.
[29] X. Ma, A. Jannasch, U.-R. Albrecht, K. Hahn, A. Miguel-López, E. Schäffer, S. Sánchez, Nano Lett. 15 (2015) 7043–7050.
[30] O.S. Wolfbeis, M. Schäferling, A. Dürkop, Microchim. Acta 143 (2003) 221–227.
[31] Y. Hitomi, T. Takeyasu, T. Funabiki, M. Kodera, Anal. Chem. 83 (2011) 9213–9216.
[32] M. Ornatska, E. Sharpe, D. Andreescu, S. Andreescu, Anal. Chem. 83 (2011) 4273–4280.
[33] C. Li, J. Hu, T. Liu, S. Liu, Macromolecules 44 (2011) 429–431.
[34] Y. Wang, X. Ma, Y. Wen, Y. Xing, Z. Zhang, H. Yang, Biosens. Bioelectron. 25 (2010) 2442–2446.
[35] M.Y. Hua, Y.C. Lin, R.Y. Tsai, H.C. Chen, Y.C. Liu, Electrochim. Acta 56 (2011) 9488–9495.
[36] H. Wang, S.-M. Park, Anal. Chem. 79 (2007) 240–245.
[37] H. Chang, J.A. Ho, Anal. Chem. 87 (2015) 10362–10367.
[38] V. Raj, R. Jaime, D. Astruc, K. Sreenivasan, Biosens. Bioelectron. 27 (2011) 197–200.